MnAs dots grown on GaN(0001̄)-(1×1) surface

I. A. Kowalik, B. J. Kowalski, R. J. Iwanowski, K. Kopalko, E. Łusakowska, and M. Sawicki

Institute of Physics, Polish Academy of Sciences, Aleja Lotników 32/46, PL-02 668 Warsaw, Poland

J. Sadowski

MAX-Lab, Lund University, SE-221 00 Lund, Sweden
and Institute of Physics, Polish Academy of Sciences, Aleja Lotników 32/46, PL-02 668 Warsaw, Poland

M. Adell

Department of Physics, Chalmers University of Technology and Göteborg University, SE-412 96 Göteborg, Sweden

I. Grzegory and S. Porowski

Institute of High Pressure Physics, Polish Academy of Sciences, Sokołowska 29, PL-01 141 Warsaw, Poland
(Received 7 March 2007; published 4 June 2007)

MnAs has been grown by means of MBE on the GaN(0001̄)-(1×1) surface. Two options of initiating the crystal growth were applied: (a) a regular MBE procedure (manganese and arsenic were delivered simultaneously) and (b) subsequent deposition of manganese and arsenic layers. It was shown that spontaneous formation of MnAs dots with the surface density of 1×10^{11} cm^{-2} and 2.5×10^{11} cm^{-2}, respectively (as observed by atomic force microscopy), occurred for the layer thickness higher than 5 ML. Electronic structure of the MnAs/GaN systems was studied by resonant photoemission spectroscopy. That led to determination of the Mn 3d-related contribution to the total density of states distribution of MnAs. It has been proven that the electronic structures of the MnAs dots grown by the two procedures differ markedly. One corresponds to metallic, ferromagnetic NiAs-type MnAs, the other is similar to that reported for half-metallic zinc-blende MnAs. Both systems behave superparamagnetically (as revealed by magnetization measurements), but with both the blocking temperatures and the intradot Curie temperatures substantially different. The intradot Curie temperature is about 260 K for the former system while markedly higher than room temperature for the latter one. Relations between growth process, electronic structure, and other properties of the studied systems are discussed. Possible mechanisms of half-metallic MnAs formation on GaN are considered.

I. INTRODUCTION

Manganese arsenide has been subjected to investigations for a century, at least, since the commonly cited paper by Heusler[1] was presented. Its coupled structural and magnetic properties attracted particular interest. At room temperature, it exists in the ferromagnetic α phase, with hexagonal NiAs structure. It transforms into the orthorombic, paramagnetic β phase by a first order phase transition at 40 °C.[2] At 130 °C, the crystalline structure of MnAs changes again to a hexagonal (NiAs-like) one and the paramagnetic γ phase is formed.[3] Interesting magnetic properties of MnAs and other manganese pnictides inspired extensive theoretical studies aimed at determination of the electronic structure and the nature of magnetism of these compounds.[4–13] The results, together with the experimental data related to the band structure,[14–16] showed that the electronic structure of MnAs and related compounds should be described in the model of itinerant d electrons with strong As 4p-Mn 3d hybridization. Owing to that, the density of electronic states at the Fermi level is relatively low in these materials. The maxima related to the Mn 3d states in ferromagnetic MnSb occur at about 2.5 eV above and 1 eV below the Fermi level.[10] Such description of the electronic structure of manganese pnictides accounts for experimental results concerning their magnetic properties and the specific heat.

Recently, MnAs and related compounds regained considerable interest in the context of emerging projects of spin-electronic (spintronic) devices. Ferromagnetic materials compatible with contemporary semiconductor technology would be particularly important for such applications.[17] Ferromagnetic layers would be indispensable in structures designed as emitters, controllers or detectors of spin-polarized currents. Ferromagnetic materials can also be applied in formation of nanomagnets as sources of local magnetic fields in spin-electronic or magnetoelectronic systems. Among ferromagnetic materials suitable for such purposes, selected compounds of Mn (like GaMn and MnAs) are considered.[18–22] Possibility of spontaneous formation of nanostructures or engineering of the layer properties by suitable selection of substrate structure and parameters would lead to even more sophisticated applications, like arrays of nanomagnets or systems of coupled ferromagnetic dots. In this context, MnAs is especially interesting, due to the coupling between its magnetic properties and structure.[23] This inspired attempts to perform overgrowth of MnAs on various substrates [e.g., Si(001),[20] GaAs(001),[24,23] GaAs(111),[25] GaMnAs,[26] ZnSe(Ref. 27)]. MnAs-based systems became important examples of so-called heteroepitaxy of dissimilar materials.[28,29] It is a technique exploiting large lattice misfit and strong strain at the interface in order to design the structure and adequate properties of the epilayer. On the other side, the

possibility of modification of the properties of MnAs induced by a choice of the substrate and deposition mode expands the range of MnAs-based systems supposed of exhibiting ferromagnetic properties. This is also important from the point of view of basic research and may lead to better understanding of mechanisms leading to magnetic interactions, previously investigated for bulk MnAs.

In this work, we have performed complex studies of the MnAs epilayers grown (by MBE) on GaN(000$\bar{1}$)-(1×1) surface, which included investigations of an influence of the growth conditions on their morphology, magnetic properties, and electronic structure. Both materials have hexagonal structure in the plane perpendicular to the *c* axis, where $a_{MnAs} > a_{GaN}$. Due to this misfit, spontaneous formation of MnAs dots in this system can be expected [contrary to the case of MnAs/GaAs(111)]. In order to verify this hypothesis, we have deposited MnAs epilayers on the (000$\bar{1}$) GaN surface under continuous *in situ* monitoring of their thickness and crystalline structure [by electron diffraction (RHEED)]. This, together with *ex situ* atomic force microscopy (AFM) results, confirmed that islands of MnAs are formed for the amount of MnAs larger than that corresponding to 5 ML. We apply two methods of growth initiation—both of them lead to dots formation. However, electronic structures probed by means of resonant photoemission spectroscopy turns out to be different. The magnetization measurements prove that the ensembles of dots exhibit superparamagnetic properties, although the blocking temperatures and the Curie temperatures characterizing these two systems differ markedly. We present analysis and comparison of the data acquired for samples grown by regular MBE procedure (some of them preliminarily presented in Ref. 30) and by the process initiated by subsequent deposition of manganese and arsenic. The use of resonant photoemission spectroscopy enables us to determine the electronic states distribution of deposited MnAs and, especially, a partial contribution provided by the Mn 3*d* electrons. The changes revealed in the electronic structure of MnAs dots and their relation to growth procedure and other properties of the investigated systems are discussed.

II. EXPERIMENTAL DETAILS

The growth of MnAs layers and their electronic structure were investigated in the National Electron Accelerator Laboratory for Nuclear Physics and Synchrotron Radiation Research (MAX-lab), Lund University, Sweden. The layers were grown on bulk GaN substrates by means of MBE technique. The GaN crystals with hexagonal crystalline structure were grown by means of a high pressure technique at the Institute of High Pressure Physics, Polish Academy of Sciences, Warsaw, Poland. The (000$\bar{1}$) surfaces of the GaN substrates used in our experiments were initially prepared by *ex situ* mechano—chemical polishing. Prior to the MnAs growth and photoemission measurements, they were introduced into the ultra high vacuum (UHV) system and subjected to an *in situ* cleaning procedure consisting of the cycles of Ar$^+$ ion bombardment and subsequent annealing at

500 °C. As previously shown,[31] such a procedure leads to a clean and well-ordered GaN(000$\bar{1}$)-(1×1) surface. In the present experiments, the surface crystallinity was assessed *in situ* by electron diffraction observations (LEED and RHEED).

The layers of MnAs were grown stepwise in a KRYO-VAK III-V MBE system directly attached to the spectrometer. The electronic structure of the system was investigated *in situ* at each stage of the growth process by means of photoelectron spectroscopy. The layer structure was assessed by RHEED (during growth in the MBE system) and LEED (in the photoelectron spectrometer) techniques. The morphology of the MnAs/GaN systems with dots formed on the surface was studied *ex situ* by AFM. The magnetic properties of this system were determined by the superconducting quantum interference device (SQUID) technique.

The photoemission experiments were carried out at the beamline 41 of MAX-lab. The overall energy resolution was kept around 150 meV, and the angular resolution was about 2°. The origin of the binding energy scale was set at the Fermi level (determined for the reference metal sample). The angle between incoming photon beam and the normal to the surface was kept at 45°. The spectra were normalized to the monochromator output and photon flux variations.

## III. RESULTS AND DISCUSSION

A. Growth and morphology

The MnAs growth process is carried out by an MBE technique with use of an As$_2$ cracker source. The GaN substrate temperature is 350 °C. The Mn flux is calibrated by measuring RHEED oscillations for GaMnAs(100) calibration samples.[32] During the growth of the MnAs samples the Mn flux corresponds to the layer growth rate of 0.8 ML/min for MnAs with the NiAs-type structure. As a consequence, in this paper we measure the amount of MnAs grown on GaN in monolayers of relaxed hexagonal MnAs.

The growth of MnAs is monitored *in situ* by RHEED. For the clean GaN(000$\bar{1}$)-(1×1) surface, a streaked pattern, characteristic of an atomically flat surface, is observed. The first layer of MnAs is grown by two different modes: with both Mn and As sources open (regular MBE growth) (I) or by an atomic layer epitaxy (ALE)-like technique (first an Mn layer is deposited then, the Mn source is shut and the As source is open) (II). Independently of the growth method, the first stages of deposition (about 1 ML) cause blurring of the RHEED pattern. Further deposition, performed in a standard MBE mode, leads to improvement of the pattern (streaks became again stronger and sharper)—then, at about 5 ML, the critical thickness is achieved and the pattern switched to a dotted one, indicative of three-dimensional (3D) growth. The mechanism of two-dimensional (2D) growth mode observed, in spite of the large lattice mismatch in the system, for the thin MnAs layers (<5 ML) on GaN seems to be similar to that described for InAs/GaAs.[33] The large lattice mismatch is partly relaxed by dislocations at the beginning of the growth process and this leads to the blurring of RHEED pattern observed for very thin layers. Further
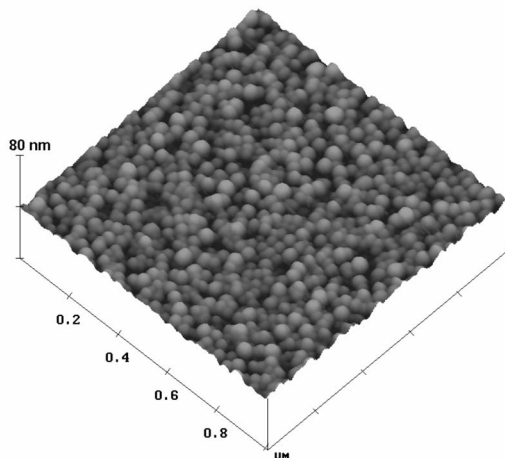
a.   MnAs(6 ML)/GaN (I)   b.   MnAs(8 ML)/GaN (II)
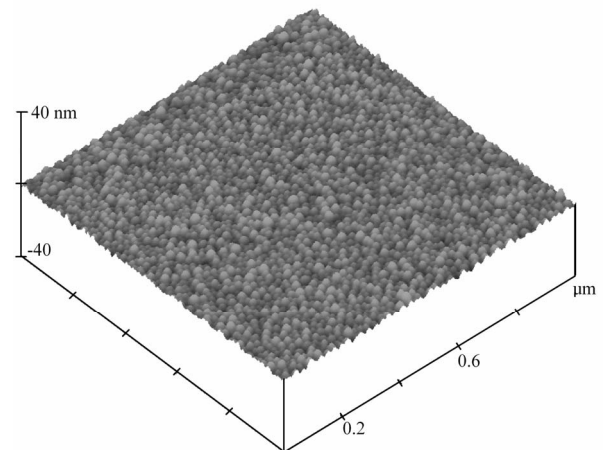
FIG. 1. The AFM images of MnAs(6 ML)/GaN(000$\bar{1}$) (I) and MnAs(8 ML)/GaN(000$\bar{1}$) (II) systems.

growth of MnAs, on top of the defected layers, results in formation of a smoother surface and the improved streaky RHEED pattern. When the epilayer becomes thicker than 5 ML, dots form on the surface.

An AFM investigation of the samples morphology confirms that MnAs dots appear (Fig. 1) for both growth procedures. The sample prepared by the regular MBE deposition (with MnAs amount equivalent to 6 ML) is denoted by I. The obtained dots have the average diameter of 40 nm. After the ALE-like initiation of the growth followed by standard MBE deposition (the sample with 8 ML of MnAs is denoted by II), the dots are somewhat smaller—they have the average diameter of 25 nm. In both cases, the average height of the dots is equal to 4 nm. However, it was proved by Sadowski *et al.*[26] that AFM markedly overestimates the size of the dots in comparison with HRTEM results. The diameter of the dots determined by AFM did not correspond to their size but was a convolution of the real dot shape and the shape and size of the AFM tip. The dot diameter derived from HRTEM in Ref. 26 was about 10 nm while that estimated from the AFM data was approximately 8 times larger. Therefore, the average density of dots seems to characterize better the dot systems and it allows reliable comparison of the results obtained by different groups. For sample I [Fig. 1(a)], the dot density is about 1×10^{11} cm^{-2}; for sample II [Fig. 1(b)], 2.5×10^{11} cm^{-2}. For comparison, MnAs dots (with zinc-blende or NiAs-type structure) on GaAs (Ref. 34) formed with the density of $1.5-3.5 \times 10^{12}$ cm^{-2}, NiAs-type MnAs dots on annealed GaMnAs (Ref. 26), 2×10^{10} cm^{-2}, zinc-blende Mn(Ga)As nanoclusters in GaAs (Ref. 35), 1×10^{10} cm^{-2}. Clearly, the density of dots shown in Fig. 1 corresponds well to the range of values reported in the literature. Thus, we expect that the real average diameter of the dots does not deviate much from 10 nm, reported for MnAs dots by Sadowski *et al.*[26] and Okabayashi *et al.*[34]

B. Resonant photoemission study

Modification of the starting stage of MnAs growth does not result in qualitative changes in the morphology of the MnAs/GaN system. However, the corresponding electronic structures revealed by photoemission spectroscopy turn out to be markedly different. These studies give us a deeper insight into the structure properties of the MnAs part of the system. Since the contribution of Mn 3d states to the electronic structure of the system is the key issue which must be discussed, resonant photoemission technique has been applied. This method enables us to resolve contribution of 3d states of transition metal atoms to the photoemission spectra against the background emission from the valence band. The resonant photoemission experiments should be carried out for photon energies close to Mn 3$p \rightarrow$ 3d transition. When the photon energy matches the energy of this intraion transition to the unoccupied states in the partly filled shell (like Mn 3d), two processes leading to different final states of the same energy may occur.

The first one is the direct photoemission from the open shell to the continuum of free electron states. The second one is a process of the discrete intraion excitation. For Mn-containing crystals one considers the following transitions:

$$\text{Mn}3d^5 + h\nu \rightarrow \text{Mn}3d^4 + e^- \tag{1}$$

and

$$\text{Mn}3p^63d^5 + h\nu \rightarrow \text{Mn}3p^53d^6. \tag{2}$$

The Mn 3$p^5$3d^6 state may autoionize, by super Coster-Kronig process, to Mn 3$p^6$3d^4+e^-. This leads to a Fano resonance[36] and a Fano-type line appears in the absorption spectra at the energy corresponding to the Mn 3$p \rightarrow$ 3d transition. As a consequence, photoemission from the open shell is resonantly increased. Therefore, the resonant photoemission is widely used for identification of the features in the photoemission spectra which can be ascribed to the emission from partly filled shells. In particular, a comparison of the spectra taken for the photon energies corresponding to the maximum (close to the resonance energy) and minimum (the
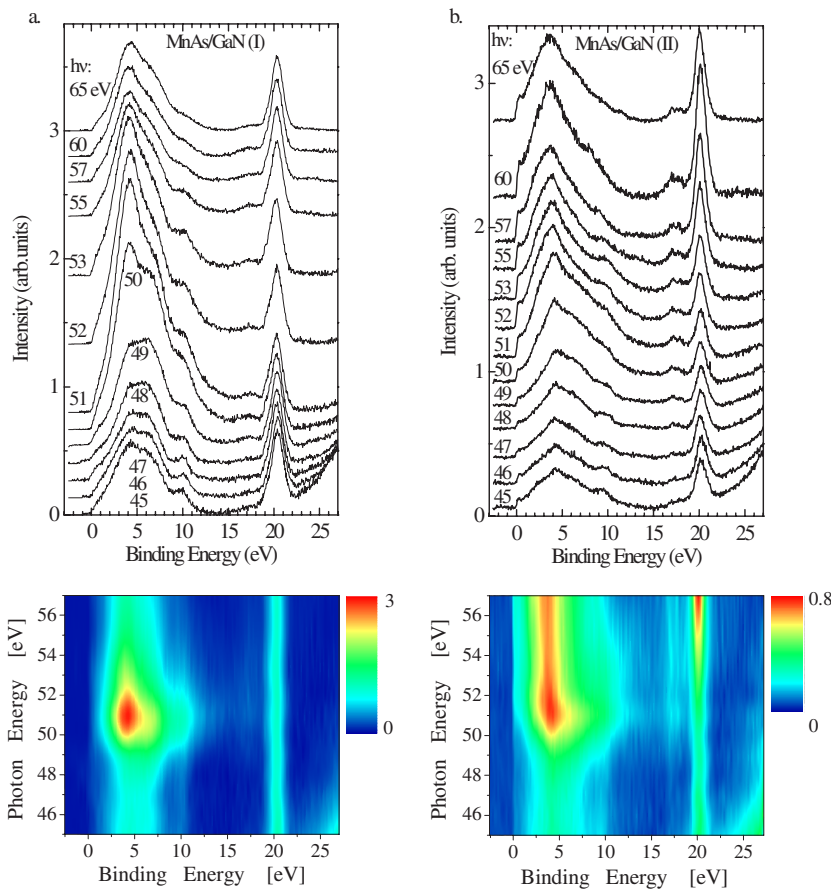
FIG. 2. (Color online) The sets of energy distribution curves obtained for type I MnAs(6 ML)/GaN(000$\bar{1}$) (a) and type II MnAs(8 ML)/GaN(000$\bar{1}$) (b) for photon energies close to Mn 3p →3d resonance.

antiresonance energy at which the emission from the open shell is suppressed) of the Fano profile clearly shows enhancement of 3d-shell-related spectral features.

Figure 2 shows sets of photoemission spectra acquired at photon energies from 45 to 65 eV (i.e., covering the photon energy of the Mn 3p→3d resonance, about 51 eV). They have been measured for both types of MnAs layers overgrown on GaN(000$\bar{1}$)-(1×1). The binding energy range of the spectra, measured with respect to the Fermi energy, corresponds to the valence band (0–12 eV) and the Ga 3d maximum (at about 20 eV). Analysis of these sets of spectra shows that the intensity of emission from the valence band is strongly sensitive to photon energy. The resonance conditions occur for about 51 eV. The spectra taken at 48 eV correspond to the antiresonance minimum of the Fano profile. Apart from these strong resonances at the same photon energies, both sets of spectra show important differences. The most important one occurs at the Fermi energy. For the sample II, the sharp edge is visible. For the sample I, the leading edge of the spectrum also starts at the Fermi energy but it is much less steep. This shows that the sample II has metallic properties, in contrast to the sample I. The overall shapes of the valence band main maxima (at about 4 eV) are also somewhat different and additional shoulders at 6 and 10 eV are clearly discernible for the sample I.

Let us turn to the maximum occurring at 20 eV. It is related to the Ga 3d core level. Its presence indicates that considerable emission from the GaN substrate contributes to the recorded spectra. It is also possible to detect differences

between interfaces formed in both structures. In particular, the additional feature appearing for the sample II at about 17 eV, just above the Ga 3d peak, suggests different interactions occurring at the interface formed between GaN and MnAs.

In order to visualize the development of the electronic structure of the MnAs/GaN system and variations occurring due to different formation of the first monolayer of MnAs we show sets of photoemission spectra acquired for the samples I and II, under resonance and antiresonance conditions, for clean GaN surface and for subsequent stages of MnAs growth (Fig. 3). The spectra obtained for clean surfaces match those previously reported for GaN crystal surfaces prepared by the same method,[31] including small variations in relative intensities of the main maximum (at about 4 eV) and the shoulder at 7 eV. According to our previous studies, it is the clean GaN(000$\bar{1}$) surface with hexagonal (1×1) symmetry, showing surface electronic structure features characteristic of regions with the relaxed clean GaN(000$\bar{1}$) surface structure as well as of those with (000$\bar{1}$):Ga configuration, covered with an additional layer of Ga atoms bound at the "on top" positions above N atoms.[31] Difference between the spectra taken under Mn 3p→3d resonance ($h\nu$=51 eV) and antiresonance ($h\nu$=48 eV) conditions for clean GaN is negligible in comparison with those observed for samples covered with MnAs, independently of the thickness. For both cases, the first two stages of MnAs growth correspond to layer thickness lower than the critical one (5 ML), the third stage corresponds to the layer transformed into dots. Marked
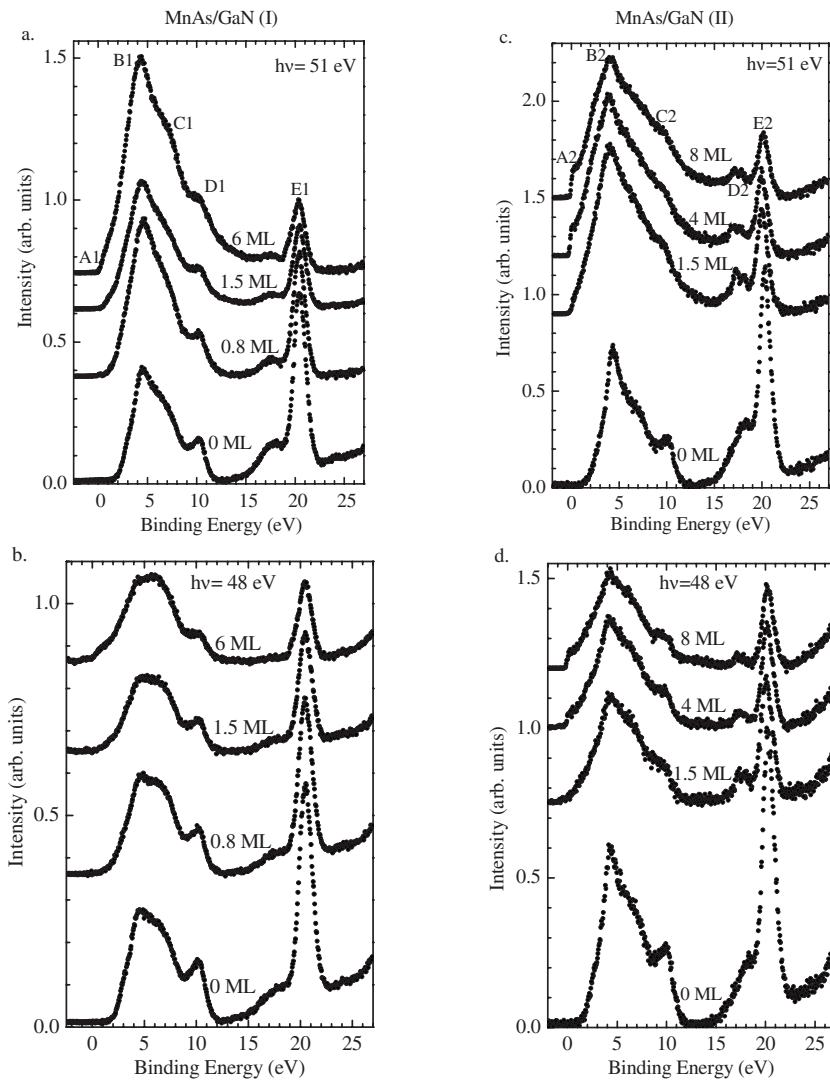
FIG. 3. Energy distribution curves taken for $h\nu$=51 eV (resonance) (a, c) and 48 eV (antiresonance) (b, d) after subsequent growth stages of type I MnAs/GaN(000$\bar{1}$) (a, b) and type II MnAs/GaN(000$\bar{1}$) (c, d) structures. MnAs coverage is indicated at the graphs.

changes in the shape of the valence band spectrum appear as soon as the first layers of MnAs have been deposited. They manifested themselves both in the resonance and antiresonance spectra. However, the main MnAs-related maximum, clearly visible in the resonance spectra, gets markedly decreased for the antiresonance case. Intensity of MnAs-related features increase with rising MnAs layer thickness, in particular for the sample I. However, MnAs dots formation does not lead to qualitative changes in the spectra. The intensity of Ga 3d core line decrease with the MnAs layer nominal thickness. However, we want to point out that the strongest change occurs after a growth of the very first MnAs layers (about 1 ML). Further growth of MnAs causes relatively weak decrease of the maximum. The Ga 3d peak is still clearly discernible for the largest amounts of MnAs (6, 8 ML). This confirms that MnAs does not form a uniform layer with constant thickness, at this stage of growth.

The main differences between the samples I and II, including the Fermi edge and the additional structure at 17–18 eV, are discernible in all spectra II for both photon energies. Intensity of the Fermi edge of the sample II increases with MnAs coverage. The feature close to the Ga 3d peak (D2) decreases together with suppression of the main

Ga 3d peak (E2) due to increasing amount of MnAs covering the GaN surface. This structure closely resembles that appearing after deposition of Mn on the GaN(000$\bar{1}$)-(1×1) surface[37]—an additional component of the Ga 3d spectral feature, at about 2 eV above the main peak. This shows that the first layer of Mn, deposited in the ALE-like process, interacts with GaN, the surface gets disrupted and a reactive, Ga-rich interface is formed. Then, the next layers of MnAs are grown and the intensity of this feature decreases. This indicates that the excessive Ga responsible for this structure remains at the interface. For the sample I, no signs of surface disruption can be discerned in the spectra. Manganese and arsenic delivered to the clean GaN surface forms MnAs layer instantly, without anterior reacting with GaN substrate.

The considerable intensity of Ga 3d peak indicates that a part of the recorded spectra originates from the GaN substrate. In order to reveal emission from the MnAs dots we subtract the spectra taken for the respective GaN substrate. Before subtraction, the spectra of GaN have been normalized in an accordance with the intensities of the Ga 3d peaks. This enables us to take into account dumping of GaN emission increasing with MnAs overgrowth. Figures 4(a) and 4(b) show results of such a procedure applied to the spectra
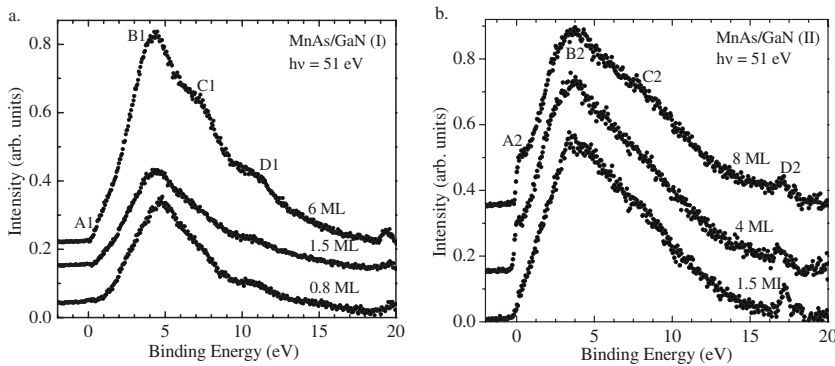
FIG. 4. Emission from MnAs—a measure of MnAs density of electronic states—revealed by subtraction of the EDCs of clean GaN from the spectra of MnAs/GaN(000$\bar{1}$) I (a) and II (b) after subsequent stages of the system formation. Curves are shifted along the intensity axis for clarity.

taken at $h\nu = 51$ eV (the resonance conditions) for the samples I and II, respectively. They correspond mainly to emission from the valence band of MnAs but some features related to modifications of the substrate surface [like the feature D2 (17.2 and 18 eV for 1.5 ML MnAs) in Fig. 4(b)] also occur. We assign them to the presence of excessive Ga at the interface due to interaction of Mn with GaN substrate.

The subtraction of the GaN substrate emission emphasizes the differences between both types of the samples indicating that MnAs systems formed on the samples I and II have markedly different character. First, a sharp edge at the Fermi energy (A2), occurs only for the sample II. Second, the main feature of the valence band is sharper for the sample I and additional shoulders can be resolved on its high binding energy slope (C1 at 7.2 and D1 at 11 eV).

We find that the overall shape of the MnAs related emission from the sample II [Fig. 4(b)] corresponds well to that of hexagonal, ferromagnetic α-MnAs. Results of calculations[12] suggested that for this phase the main maximum of the spectrum occurred at about 2 eV below the Fermi edge. However, photoemission experiments carried out for epilayers of hexagonal MnAs clearly showed that the main maximum of the spectrum taken for photon energy close to Mn $3p \rightarrow 3d$ resonance should occur at about 4 eV below the clearly discernible, sharp Fermi edge.[26,34,38,39] This shape of the spectrum is indicative for metallic character of the system with relatively high density of states at the Fermi energy.

The shape of the spectra of the sample I seems to correspond to those reported for systems of dots of zinc-blende MnAs.[34,40] In particular, similarity of the energy position of the main maximum, very low emission intensity at the Fermi energy and additional shoulders appearing in the spectra obtained by Ono *et al.*,[40] Okabayashi *et al.*[34] and in this work justify this observation.

However, according to the literature, the zinc-blende structure of MnAs dots,[34,40] or even layers,[41] were stabilized by zinc-blende GaAs substrate. As Moreno *et al.*[35] and Okabayashi *et al.*[34] showed, zinc-blende structure was sustained only in very small MnAs clusters or dots, with diameter of less that 10 nm [as measured by high-resolution transmission electron microscopy (HRTEM)]. Larger MnAs dots had NiAs-type structure.[26,34,35] Since the GaN substrate has hexagonal structure, this mechanism cannot lead to the formation of zinc-blende MnAs dots on the sample I. Besides, the dots on the sample I are larger than those on the sample II (with NiAs-type structure).

The photoelectron spectroscopy probes directly the electronic states distribution in the system but not its crystallographic structure. Therefore, the results reported in this paper cannot prove whether the dots have zinc-blende structure or NiAs-type structure. Unfortunately, common x-ray diffraction methods do not give conclusive results for so thin MnAs structures.[42] However, it was shown by theoretical calculations that half-metallic electronic structure with the Fermi level lying in the energy band gap of the minority-spin bands is likely to occur in zinc-blende MnAs (Refs. 43–46), as well as in other manganese pnictides.[46,47] Distortions of the crystal structure may also influence band structure of these materials and their magnetic properties. Tetragonal distortions of zinc-blende structure in MnSb or MnBi support half-metallicity and ferromagnetism[47] or, in MnAs/Si, such distortions induce transition to ferromagnetism and half-metallicity.[45] In contrast to that, for hexagonal MnAs, Debernardi *et al.*[48,49] showed that uniaxial stress in NiAs-type MnAs (related to pseudomorfic growth on a lattice mismatched substrate) led to some nonlinear changes in electronic and magnetic properties, but they did not result in half-metallic electronic band structure. Therefore, formation of MnAs with zinc-blende crystallographic structure still seems to be a necessary condition for occurrence of half-metallic band structure in the system. However, such an interpretation of our results needs confirmation that a cubic phase of the hexagonal crystal can grow on the hexagonal substrate.

We believe that tentative arguments for it can be derived from a phenomenon reported by Kitamura *et al.*[50] for InGaN epilayers grown on InN. For In contents below 0.66, a cubic phase appeared in the InGaN epilayers thicker than a critical thickness. That was ascribed to degradation of the crystalline quality due to an abrupt change in the crystal composition at the interface. MnAs/GaN would be another system in which such phenomenon could occur. We postulate that differences in initial growth stages of the samples I and II and different interactions between Mn and the GaN substrate lead to different crystalline structures of the overgrown MnAs. The interface of the sample I seems to be more abrupt due to the absence of interaction between components of MnAs and the GaN substrate. If this promotes cubic phase of MnAs formation, half-metallic electronic structure may occur and manifest itself in the reported photoemission experiments. Confirmation of this suggestion needs further studies, in particular crystal structure investigations by means of surface sensitive methods.
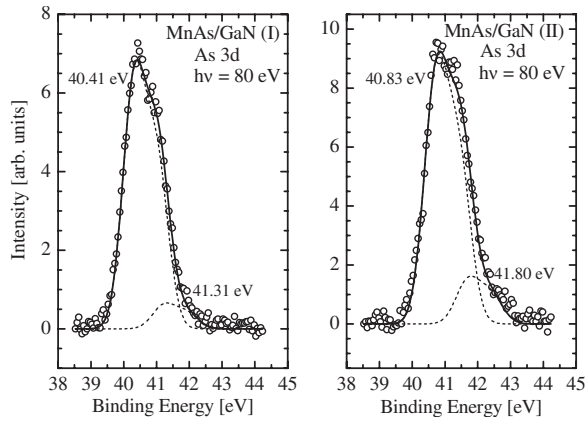
FIG. 5. The As $3d$ feature measured for MnAs(6 ML)/GaN(000ī) (I) and MnAs(8 ML)/GaN(000ī) (II) shown together with the results of deconvolution into spin-orbit split dublets of Gaussians.

The next argument for the difference between structures of MnAs(I) and MnAs(II) arises from the photoelectron spectroscopy of the As $3d$ core level. In order to reveal the energy shifts of this core level, reflecting changes in chemical bonding and structure of MnAs, As $3d$ maxima have been recorded at $h\nu = 80$ eV for both systems (Fig. 5). For the energy scale with origin at the Fermi energy, the Ga $3d$ peaks of the samples I and II were aligned well but for the As $3d$ feature an energy shift of about 0.4 eV clearly occurred. The same energy position of the Ga $3d$ peak observed for both samples proved that surface conditions on them are similar. The energy shift of the As $3d$ feature can be
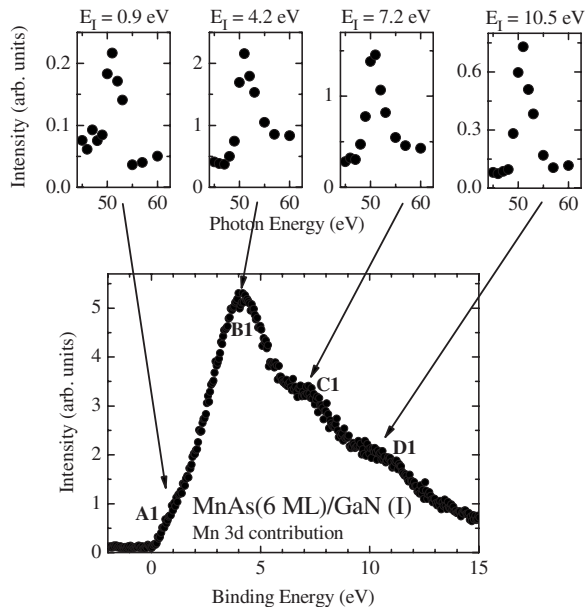

FIG. 6. Difference spectrum—a measure of Mn $3d$ contribution to the valence band—obtained by subtraction of the antiresonance spectra ($h\nu = 48$ eV) from the resonance spectra ($h\nu = 51$ eV) for type I MnAs/GaN(000ī). Constant-initial-state spectra were made for the initial-state binding energies corresponding to the main features of the difference spectrum.

FIG. 7. Difference spectrum obtained by subtraction of the antiresonance spectra ($h\nu = 48$ eV) from the resonance spectra ($h\nu = 51$ eV) for type II MnAs/GaN(000ī). Constant-initial-state spectra were made for the initial-state binding energies corresponding to the main features of the difference spectrum.
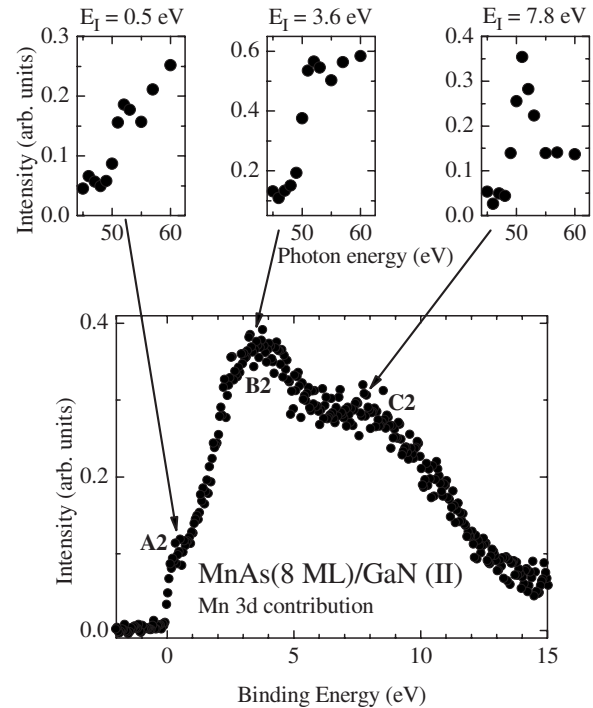
interpreted as a manifestation of a different structure of the MnAs layers, consistent with differences revealed in the MnAs valence band shape.

Each of the As $3d$ features can be decomposed into two Gaussian dublets corresponding to As $3d_{5/2}$ and As $3d_{3/2}$ with spin-orbit splitting of 0.7 eV.[51,52] The dublets are separated by about 0.9 eV. The second one, at the higher binding energy, is markedly weaker and corresponds to 10%–15% of the total intensity of the As $3d$ feature, for both systems. Similar energy separation and relative intensity occurred for thinner MnAs layers. Therefore, we cannot interpret the minor component as corresponding to surface As atoms. Moreover, we could expect that surface related contribution to the As $3d$ maximum would be shifted to lower binding energies with respect to the bulk related one, like in GaAs.[51–53] Similarly, this feature cannot correspond to As atoms in a different lattice position or chemical state. It is hardly possible that relative populations of As atoms in different states are independent from the MnAs layer thickness, structure, and morphology. Thus, we can only interpret it tentatively as a satellitelike structure.

Further information confirming the difference between electronic structures of the two investigated MnAs systems has been obtained thanks to one of the most important advantages of resonant photoemission spectroscopy—its enhanced sensitivity to emission from open shells of transition elements. Figures 6 and 7 show difference spectra obtained by subtraction of curves obtained for antiresonance photon energy from those taken under resonance conditions. In such spectra which measure Mn $3d$ contribution to the valence
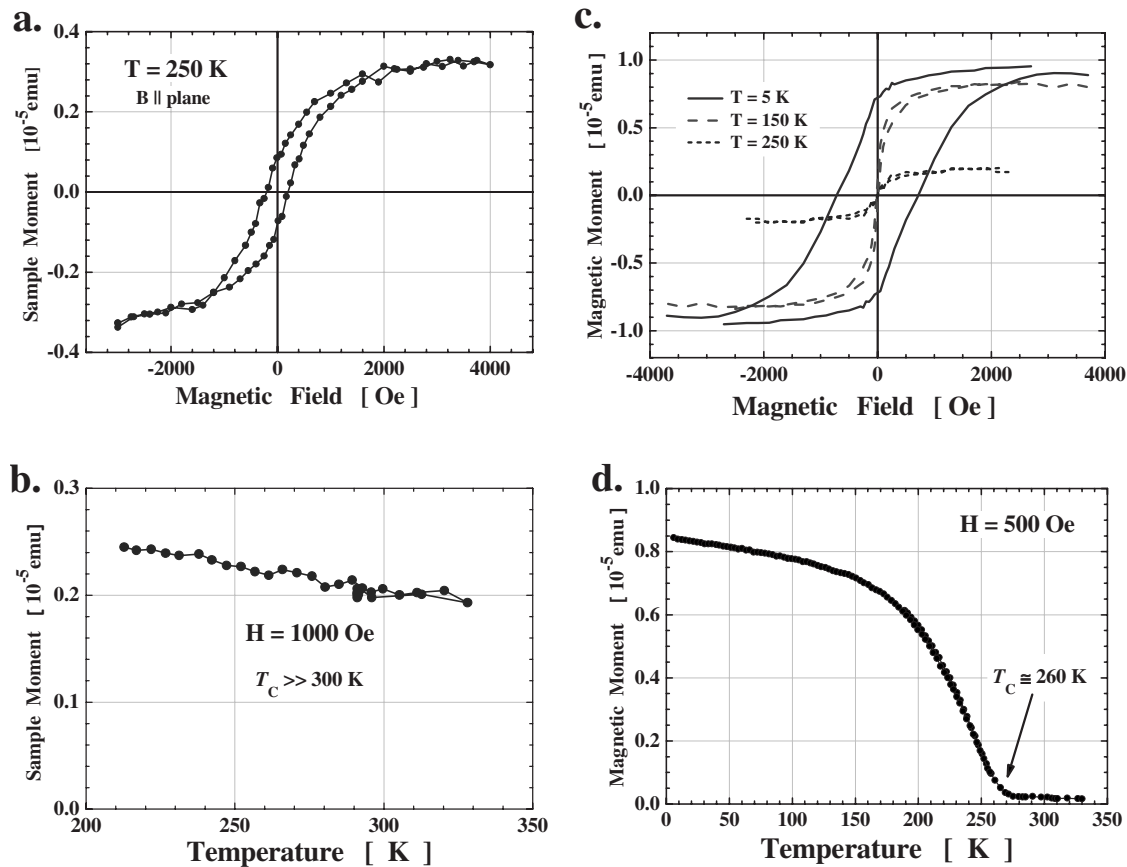
FIG. 8. Magnetic moment of type I (a,b) and type II (c,d) MnAs nanodots. Diamagnetic (linear in field) GaN substrate signal has been subtracted for the data.

band, the main differences between the samples I and II manifested themselves even more discernibly. Consistently with the results of the data analysis presented above, the curve obtained for the sample I is very similar to the difference spectra of zinc-blende MnAs dots, reported by Ono *et al.*[40] Only the shoulder at 7.2 eV is more pronounced in our spectrum.

The differences between MnAs type I and type II manifest themselves explicitly in the constant-initial-state (CIS) photoemission spectra (Figs. 6 and 7). They show photoemission intensity (relevant GaN substrate emission subtracted) as a function of photon energy for the initial-state binding energies corresponding to the main features of the difference (resonance-antiresonance) spectra. For the sample I (Fig. 6), the curves obtained for four features at 0.9, 4.2, 7.2, and 10.5 eV differ in intensity but a sharp maximum at the same photon energy can easily be seen in each of them. For the sample II (Fig. 7), a sharp peak occurs only in the CIS curve corresponding to the shoulder at 7.8 eV. For the main maximum and the shoulder just below the Fermi edge, only very weak features on a nonresonant background appear. This set of CIS spectra corresponds well to those reported for the systems exhibiting in photoemission a strongly resonant satellite and an almost nonresonant main line, like Ni.[54] Such character of photoemission spectrum is interpreted as a manifestation of two different final states occurring in the system. The main line corresponds to a final state fully screened in the *d* shell, while the satellite corresponds to that screened by

band electrons (4*s* in nickel). However, the CIS spectra of sample I can be compared with those of many Mn compounds, like $MnCl_2$ (Ref. 55) or diluted magnetic semiconductors with Mn.[56] For those systems, Fano-like lines with distinct maxima were observed in CIS spectra throughout the *d*-shell related difference spectrum. Analysis of the results collected for various transition-metal-containing compounds showed that the appearance of a resonant satellite with a nonresonant main line in the spectra corresponded to large configuration interaction or strong mixing of *d* and ligand states in the system.[57] Thus, we can expect that similar difference in these characteristics occurs also in samples I and II. This supports our supposition that the surroundings of Mn atoms in the investigated systems differ substantially.

C. Magnetic properties

Magnetic properties of the MnAs dots are investigated in a homemade SQUID magnetometer. Figure 8 shows the magnetic field, $m(H)$, and the temperature dependence, $m(T)$, of the net magnetic moment of both types of MnAs structures. All the measurements are performed with the magnetic field applied in the plane of the samples. Both systems exhibit strong nonlinear magnetic field response even at high temperatures and show a development of coercivity and remanence on lowering *T*. It is, however, important to stress here that neither of these, nor even the clear saturation of the magnetization, can be taken as an indication of a presence of

a uniform ferromagnetic state. On the contrary, the characteristic rounded shape of $m(H)$ curves (Langevin function alike) suggests that we deal with predominantly superparamagnetic behavior of an ensemble of ferromagnetic particles, but the small magnetic remanence (or coercivity) indicates a presence of strong enough magnetic anisotropy to block (at least partially) some of the particles even at temperatures as high as 250 K. Therefore, an external nonzero magnetic field is required to flip the moments of those nanodots which were trapped behind the energy barrier for their magnetization reversal: $\Delta E = KV$, where V is the particle volume, and K is the relevant magnetic anisotropy energy density. This leads to nonzero coercivity and remanence, resulting in an open magnetic hysteresis of the system. The maximum temperature at which, on the time scale of the experiment, the statistically significant number of magnetic moments remains blocked is called the blocking temperature, T_B, however, minute blocking effects can persist to much higher temperatures, T_B^{max}, if the particle size and/or anisotropy distribution is particularly large. We note that, a similar behavior can be brought about if there exists a substantial magnetic coupling between the particles. However, as observed here, the varying width of the $m(H)$ curves, with the most narrow point at the magnetization reversal [seen particularly in Fig. 8(c)] indicates strongly the dominance of activated processes related to the existence of the barriers over the mutual magnetic coupling in the investigated nanodots systems.

It is widely accepted that for a system of identical noninteracting particles the following relationship defines T_B:

$$T_B \simeq KV/25k_B \tag{3}$$

and so for real systems a maximum temperature in which blocking effects are observed serves as an upper limit for the KV product. Alternatively, knowing K or V beforehand, the relationship allows to evaluate the other. As argued in Sec. III A, an average MaAs dot diameter is expected to be 10 nm. We can independently confirm this finding by fitting the Langevin function to the 250 K data for type II hexagonal MnAs dots, for which a near perfect superparamagnetic behavior is seen. An excellent fit [not shown for clarity on Fig. 8(c)] is obtained assuming an effective magnetic moment $\mu = 40\,000\mu_B$ for each MnAs dot. Since at 250 K MnAs saturation magnetization is approximately $2\mu_B$ per Mn atom, the effective "magnetic" volume of an average MnAs nanodot approximates to 1000 nm^3, giving the lateral size of 10 nm, as deduced from AFM studies. Now employing Eq. (3) we arrive at $K \simeq 1 \times 10^5$ erg/cm^3 required to reproduce T_B of 200 K as results in Fig. 8(c) suggest. This is a rather large value for K laying between anisotropy constants of iron (cubic) and cobalt (uniaxial), and is approximately 20 times that of bulk MnAs (uniaxial).[58] But such a discrepancy can by no means devalue the proposed analysis. As argued above, this is the upper limit for K, with no solid indication of how many times the target is overshot. It is also important to keep in mind that the nanodots we investigate are formed only owing to a large epitaxial and/or misfit strain, and its presence is expected to augment the magnetic anisotropy substantially.

A similar analysis for type I nanodots is largely precluded since we do not possess any $m(H)$ dependency for this system in the pure superparamagnetic regime, see Fig. 8(a). It is likely that for these nanodots the blocking temperature is comparable with, or even greater than their intradot Curie temperature, T_C, approximated later to a value rather closer to 400 K than to typical 313 K for free-standing bulk MnAs. One of the reasons for such an enlargement of T_B can be a larger volume of these dots. We recall here that the AFM morphology studies suggest their 2.5 smaller surface density that can be translated into 4 times greater average volume than for the type II nanodots. Now, taking similarly enlarged magnetic anisotropy, T_B values of even a few hundred K can be easily accounted for. The contribution considered in Ref. 30 of hypothetic manganese compounds with a very high T_C, formed at the interface, can be excluded because they would manifest themselves even stronger in the sample II, with interaction of Mn with GaN clearly revealed by spectroscopy of the Ga 3d core level.

Because the structures behave superparamagnetically, neither the upper temperature limit for the nonzero coercive force (T_B^{max}) nor the vanishing of the remnant magnetization is an appropriate measure of the intradot T_C, which on the account of the data presented in Figs. 8(a) and 8(c) obviously must be higher than any of these estimates. To determine T_C we investigate $m(T)$ dependency at nearly saturating magnetic field, see Figs. 8(b) and 8(d). The two different field values used in these experiments are compromised to satisfy both the requirements to be significantly close to saturation and to minimize increasing with the applied field noise in the magnetometer. Under these experimental conditions the magnetization for type I MnAs dots remains clearly nonzero up to the highest available temperature in our magnetometer. Additionally, its very weak temperature dependence indicates rather high, substantially above 330 K, intradot T_C, so exceeding considerably that of the bulk MnAs (313 K). Markedly different behavior is seen for the second structure. Here, in the whole temperature range, the nearly saturated magnetization follows reasonably well the Brillouin function, yielding the intradot T_C only of about 260 K. In turn, this value is considerably lower than that for the bulk MnAs. Although we cannot propose a convincing microscopic argument accounting for such a huge, at least 100 K difference in T_C, we note that similarly enlarged intradot T_C values for zinc-blende MnAs nanodots can be inferred from Ono et al.[40] and Moreno et al.[35] magnetic data,[59] despite the different substrate-host matrix in their studies. So, this seems to be a common feature for zinc-blende MnAs dots. For the hexagonal, type II MnAs nanodots, a T_C lowering seems to be connected with layer-to-(nano-)dots transition and a smaller size of these dots. Most likely, an increased number of surface moments in comparison to the inside ones in the smaller dots reduces the overall strength of the magnetic coupling, resulting in noticeable T_C lowering.

IV. CONCLUSIONS

MnAs dots have been grown on the GaN(000$\bar{1}$)-(1×1) surface by means of MBE. The dots form spontaneously in

the layers thicker than 5 ML. Two methods of growth initiation have been tested: regular MBE and ALE-like (with noticeable reaction between manganese and GaN substrate). The structures grown by these methods have similar morphology but markedly different electronic structures. The ALE-like procedure leads to the electronic structure characteristic of ferromagnetic NiAs-type MnAs. The regular MBE growth of the layer results in the density of states distribution suggesting half-metallic character of the MnAs dots. Magnetization measurements revealed further differences between the systems under investigation. Both of them exhibit superparamagnetic properties but the basic parameters describing them are considerably different. For MnAs(II), the blocking temperature, deduced from the $m(H)$ curves, is about 200 K, the intradot T_C is about 260 K. For MnAs(I), such temperatures are markedly higher than 330 K. The upper-limit value for the anisotropy energy density (K) required to reproduce experimental results for MnAs(II) turned out to be unexpectedly much higher than that characteristic of bulk MnAs, probably due to the presence of large strain in the investigated dots.

Modification of the initial stage of MnAs layer growth on GaN turns out to be an effective method for changing electronic and magnetic properties of the system. Our results suggest that MnAs/GaN is a system for which an attempt to obtain a combination of half-metallic electronic structure and T_C higher than room temperature could be reasonable. In such a material, spin-polarized currents can be effectively induced and it would be particularly useful for fabrication of spintronic devices.

ACKNOWLEDGMENTS

[1] F. Heusler, Angew. Chem. **17**, 260 (1904).

[2] R. D. Blois and D. Rodbell, Phys. Rev. **130**, 1347 (1963).

[3] B. Wills and H. Rooksby, Proc. Phys. Soc. London, Sect. B **67**, 290 (1954).

[4] J. Goodenough, *Magnetism and the Chemical Bond* (Interscience, New York, 1963).

[5] W. Albers and C. Haas, Phys. Lett. **8**, 300 (1964).

[6] K. Bärner, Phys. Status Solidi B **84**, 385 (1977).

[7] L. Sandratskii, R. Egorov, and A. Berdyshev, Phys. Status Solidi B **103**, 511 (1981).

[8] R. Podloucky, J. Magn. Magn. Mater. **43**, 204 (1984).

[9] R. Podloucky, Solid State Commun. **50**, 763 (1984).

[10] R. Coehoorn and R. de Groot, J. Phys. F: Met. Phys. **15**, 2135 (1985).

[11] K. Motizuki, J. Magn. Magn. Mater. **70**, 1 (1987).

[12] M. Shirai and Y. Tokioka, J. Electron Spectrosc. Relat. Phenom. **88-91**, 357 (1998).

[13] P. Ravindran, A. Delin, P. James, B. Johansson, J. M. Wills, R. Ahuja, and O. Eriksson, Phys. Rev. B **59**, 15680 (1999).

[14] J. Bouwma and C. Hass, Phys. Status Solidi B **56**, 299 (1973).

[15] K. Liang and T. Chen, Solid State Commun. **23**, 975 (1977).

[16] T. Chen, W. Stutius, J. Allen, and G. Stewart, in *Magnetism and Magnetic Materials*, edited by J. Becker, G. Lander, and J. Ryne, AIP Conf. Proc. No. 29 (AIP, New York, 1976), p. 532.

[17] G. Prinz, Science **250**, 1092 (1990).

[18] M. Tanaka, J. Harbison, T. Sands, B. Philips, T. Cheeks, J. D. Boeck, L. Florez, and V. Keramidas, Appl. Phys. Lett. **63**, 696 (1993).

[19] G. Kioseoglou, S. Kim, Y. Soo, X. Chen, H. Luo, Y. Kao, Y. Sasaki, X. Liu, and J. Furdyna, Appl. Phys. Lett. **80**, 1150 (2002).

[20] K. Akeura, M. Tanaka, M. Ueki, and T. Nishinaga, Appl. Phys. Lett. **67**, 3349 (1995).

[21] M. Tanaka, K. Saito, and T. Nishinaga, Appl. Phys. Lett. **74**, 64 (1999).

[22] M. Ramsteiner, H. Y. Hao, A. Kawaharazuka, H. J. Zhu, M. Kästner, R. Hey, L. Däweritz, H. T. Grahn, and K. H. Ploog, Phys. Rev. B **66**, 081304(R) (2002).

[23] A. Ney *et al.*, Phys. Rev. B **69**, 081306(R) (2004), and references therein.

[24] M. Tanaka, J. Harbison, M. Park, Y. Park, T. Shin, and G. Rothberg, Appl. Phys. Lett. **65**, 1964 (1994).

[25] J. Sadowski, J. Kanski, L. Ilver, and J. Johansson, Appl. Surf. Sci. **166**, 247 (2000).

[26] J. Sadowski *et al.*, Appl. Phys. Lett. **87**, 263114 (2005).

[27] J. Berry, S. Chun, K. Ku, N. Samarth, I. Malajovich, and D. Awschalom, Appl. Phys. Lett. **77**, 3812 (2000).

[28] K. Ploog, Mater. Sci. Semicond. Process. **4**, 451 (2001).

[29] A. Trampert, Physica E (Amsterdam) **13**, 1119 (2002).

[30] B. J. Kowalski, I. A. Kowalik, R. J. Iwanowski, E. Lusakowska, M. Sawicki, J. Sadowski, I. Grzegory, and S. Porowski, Acta Phys. Pol. A **105**, 645 (2004).

[31] B. J. Kowalski, R. J. Iwanowski, J. Sadowski, I. A. Kowalik, J. Kanski, I. Grzegory, and S. Porowski, Surf. Sci. **548**, 220 (2004).

[32] J. Sadowski, J. Z. Domagała, J. Bąk-Misiuk, S. Kolesnik, M. Sawicki, K. Świątek, J. Kanski, L. Ilver, and V. Ström, J. Vac. Sci. Technol. B **18**, 1697 (2000).

[33] H. Åsklund, L. Ilver, J. Kanski, S. Mankefors, U. Södervall, and J. Sadowski, Phys. Rev. B **63**, 195314 (2001), and references therein.

[34] J. Okabayashi, M. Mizuguchi, K. Ono, M. Oshima, A. Fujimori, H. Kuramochi, and H. Akinaga, Phys. Rev. B **70**, 233305 (2004).

[35] M. Moreno, A. Trampert, B. Jenichen, L. Däweritz, and K. Ploog, J. Appl. Phys. **92**, 4672 (2002).

[36] U. Fano, Phys. Rev. **124**, 1866 (1961).

[37] I. A. Kowalik, B. J. Kowalski, B. A. Orlowski, E. Lusakowska, R.

J. Iwanowski, S. Mickevicius, R. Johnson, I. Grzegory, and S. Porowski, Surf. Sci. **566-568**, 457 (2004).

[38] K. Shimada, O. Rader, A. Fujimori, A. Kimura, K. Ono, N. Kamakura, A. Kakizaki, M. Tanaka, and M. Shirai, J. Electron Spectrosc. Relat. Phenom. **88-91**, 207 (1998).

[39] K. Shimada, O. Rader, A. Fujimori, A. Kimura, K. Ono, N. Kamakura, A. Kakizaki, M. Tanaka, and M. Shirai, J. Electron Spectrosc. Relat. Phenom. **101**, 383 (1999).

[40] K. Ono, J. Okabayashi, M. Mizuguchi, M. Oshima, A. Fujimori, and H. Akinaga, J. Appl. Phys. **91**, 8088 (2002).

[41] T. Kim, H. Jeon, T. Kang, H. Lee, J. Lee, and S. Jin, Appl. Phys. Lett. **88**, 021915 (2006).

[42] W. Paszkowicz (private communication).

[43] M. Shirai, T. Ogawa, I. Kitagawa, and N. Suzuki, J. Magn. Magn. Mater. **177-181**, 1383 (1998).

[44] Y.-J. Zhao, W. T. Geng, A. J. Freeman, and B. Delley, Phys. Rev. B **65**, 113202 (2002).

[45] M. Kim and A. Freeman, Appl. Phys. Lett. **85**, 4983 (2004).

[46] H.-M. Hong, Y.-J. Kang, J. Kang, E.-C. Lee, Y.-H. Kim, and K. J. Chang, Phys. Rev. B **72**, 144408 (2005).

[47] J.-C. Zheng and J. W. Davenport, Phys. Rev. B **69**, 144415 (2004).

[48] A. Debernardi, M. Peressi, and A. Baldereschi, Comput. Mater. Sci. **27**, 175 (2003).

[49] A. Debernardi, M. Peressi, and A. Baldereschi, Mater. Sci. Eng., C **23**, 1059 (2003).

[50] T. Kitamura, X.-Q. Shen, M. Sugiyama, H. Nakanishi, M. Shimizu, and H. Okumura, Jpn. J. Appl. Phys., Part 1 **45**, 57 (2006).

[51] D. E. Eastman, T.-C. Chiang, P. Heimann, and F. J. Himpsel, Phys. Rev. Lett. **45**, 656 (1980).

[52] M. Prietsch, C. Laubschat, M. Domke, and G. Kaindl, Phys. Rev. B **38**, 10655 (1988).

[53] A. Chaika, V. Grazhulis, A. Ionov, S. Molodtsov, and C. Laubschat, Appl. Surf. Sci. **143**, 277 (1999).

[54] J. Barth, G. Kalkoffen, and C. Kunz, Phys. Lett. **74A**, 360 (1979).

[55] A. Kakizaki, K. Sugeno, T. Ishii, H. Sugawara, I. Nagakura, and S. Shin, Phys. Rev. B **28**, 1026 (1983).

[56] L. Ley, M. Taniguchi, J. Ghijsen, R. L. Johnson, and A. Fujimori, Phys. Rev. B **35**, 2839 (1987).

[57] L. Davis, J. Appl. Phys. **59**, R25 (1986), and references therein.

[58] K. Ploog, L. Däweritz, R. Engel-Herbert, and T. Hesjedal, Phys. Status Solidi A **203**, 3574 (2006).

[59] In Refs. 35 and 40 Curie temperature was assessed from the upper temperature limit from either nonzero remnant magnetization or nonzero coercivity, respectively. As argued in this paragraph this is at the best only the lower limit for the intraparticle (dot) T_C, particularly if the particles are randomly oriented and strained by the host environment. Indeed if our arguments are applied, the above-mentioned experiments yield much higher values of T_C.